AGU PUBLICATIONS

JGR

Journal of Geophysical Research: Oceans

RESEARCH ARTICLE

10.1002/2017JC013298

Key Points:
- Eddies from the East Australian Current have alternating upward and downward cells in their interior
- Upward and downward cells are induced by change in eddy isotropy
- Change in sea level anomaly is a good proxy for change in eddy isotropy

Supporting Information:
- Supporting Information S1

Correspondence to:
G. S. Pilo,
Gabriela.SemoliniPilo@utas.edu.au

Citation:
Pilo, G. S., Oke, P. R., Coleman, R., Rykova, T., & Ridgway, K. (2018). Patterns of vertical velocity induced by eddy distortion in an ocean model. *Journal of Geophysical Research: Oceans*, *123*, 2274–2292. https://doi.org/10.1002/2017JC013298

Received 21 JUL 2017
Accepted 26 FEB 2018
Accepted article online 7 MAR 2018
Published online 30 MAR 2018

Patterns of Vertical Velocity Induced by Eddy Distortion in an Ocean Model

Gabriela S. Pilo[1,2], Peter R. Oke[2], Richard Coleman[1,3], Tatiana Rykova[2], and Ken Ridgway[2]

[1]Institute for Marine and Antarctic Studies, University of Tasmania, Hobart, Tas, Australia, [2]CSIRO Oceans and Atmosphere Flagship, Hobart, Tas, Australia, [3]Antarctic Climate and Ecosystems CRC, Hobart, Tas, Australia

Abstract Vertical motions within eddies play an important role in the exchange of properties and energy between the upper ocean and the ocean interior. Here we analyze alternating upward and downward cells in anticyclonic eddies in the East Australian Current region using a global eddy-resolving model. The cells explain over 50% of the variance of vertical velocity within these eddies. We show that the upward and downward cells relate to eddy distortion, defined as the change in eddy shape over time. In anticyclonic eddies in the Southern Hemisphere, an inward distortion is associated with upward motion and an outward distortion is associated with downward motion. We discuss two mechanisms that link eddy distortion to vertical velocity. One mechanism relates to changes in stratification and relative vorticity in the eddy interior. The other mechanism relates to divergence of the horizontal flow in different quadrants of the eddy. We show that mesoscale changes in sea level anomaly can be used to infer the vertical motion within eddies.

1. Introduction

Vertical velocities within ocean eddies play an important role in the exchange of properties between the ocean surface and the ocean interior (e.g., Nurser & Zhang, 2000; Roemmich & Gilson, 2001), and in ecological and biogeochemical processes (e.g., Gaube et al., 2013; Klein & Lapeyre, 2009; McGillicuddy et al., 1998; Siegel et al., 2011). The upward motion within eddies promotes primary productivity, by uplifting high-nutrient waters from the ocean interior to the euphotic zone (e.g., Chelton, 2013; McGillicuddy et al., 1998). The downward motion within eddies exports tracers out of the euphotic zone and into the deep ocean (e.g., Klein & Lapeyre, 2009; McGillicuddy et al., 2003).

Despite its relevance, the vertical circulation within eddies has received less attention than other aspects of eddy dynamics. This is mostly because the vertical velocity in the ocean cannot easily be directly measured. Therefore, studies of vertical velocity within eddies rely on indirect diagnostics through the Omega equation (e.g., Martin & Richards, 2001; Nardelli, 2013; Pollard & Regier, 1992; Tintoré et al., 1991) and other methods (Strass, 1994). These diagnostics, however, require observations with high spatial and temporal resolution—both hard to achieve when observing mesoscale eddies (Allen et al., 2001; Martin & Richards, 2001). Another way to study the vertical circulation in the ocean is by analyzing the output of numerical models (e.g., Flierl & Mied, 1985; Pallas-Sanz & Viudez, 2007; Viudez & Dritschel, 2003). Modeled vertical velocity, however, cannot be easily validated against observations, and results from idealized simulations are not always applicable to real ocean eddies.

Due to the difficulties in studying vertical circulation in the ocean, McGillicuddy and Robinson (1997) and McGillicuddy et al. (1998) propose an indirect method to estimate vertical advection by mesoscale eddies—the eddy pumping mechanism. This mechanism is most relevant during the formation and strengthening of eddies, and it relates the vertical movement of isopycnals to the vertical velocity in the eddy center. The eddy pumping mechanism, however, has led to the misconception that cyclonic eddies are always upwelling and anticyclonic eddies are always downwelling. In fact, the terms "upwelling eddy" and "downwelling eddy" have been widely cited in the specialized literature (e.g., Alpine & Hobday, 2007; Nemcek et al., 2008; Oliver & Holbrook, 2014; Paterson et al., 2007; Tilburg et al., 2002; Uysal, 2006). The dominant upward or downward motion within eddies promoted by eddy pumping is a simplified view—patterns of vertical velocity within eddies are more complicated than that.

Besides the eddy pumping mechanism, the vertical circulation within eddies is also affected by eddy propagation (McGillicuddy et al., 1995), submesoscale processes (e.g., Brannigan, 2016; Lévy et al., 2001; Mahadevan et al., 2008), eddy interactions with the surrounding environment, as the wind (e.g., Dewar & Flierl, 1987; Gaube et al., 2015; Martin & Richards, 2001; Siegel et al., 2011; Stern, 1965), the ocean floor (e.g., Oke & Griffin, 2011), and other eddies (e.g., Pidcock et al., 2013), and eddy perturbation (Martin & Richards, 2001; Nardelli, 2013; Viudez & Dritschel, 2003). Here we focus on the effect of eddy perturbation in the vertical circulation.

The perturbation of the geostrophic balance of eddies induces alternating upward and downward cells that rotate around the eddy (Martin & Richards, 2001; Nardelli, 2013; Viudez & Dritschel, 2003). The nature, duration, and intensity of the perturbation dictate the number and strength of the vertical velocity cells (Martin & Richards, 2001). These cells extend radially from the eddy center to its perimeter. The changes in the eddy dynamics that link the perturbation of the eddy geostrophic balance to the alternating upward and downward cells still require further investigation. Nardelli (2013) provides indications that the basic dynamics of the alternating upward and downward cells relate to the propagation of vortex Rossby waves around the eddy (McWilliams et al., 2003). The author notes, however, that a complete characterisation of the eddy dynamics is complex.

Eddies are most intense and abundant close to western boundary currents (WBCs; Fu et al., 2010; Olson, 1991; Wyrtki et al., 1976). There, eddies often interact with other eddies and with the mean flow (Biastoch & Krauss, 1999; Bowen et al., 2005; Mata et al., 2006; Rocha et al., 2014; Waterman & Jayne, 2011). Because of these interactions, the geostrophic balance of these eddies is perturbed. Hence, the ageostrophic vertical circulation is expected to be stronger within eddies close to WBCs than within eddies in other oceanic regions.

In the East Australian Current (EAC), the WBC of the South Pacific, there has been several studies on the properties and dynamics of eddies (e.g., Roughan et al., 2017; Rykova et al., 2017; Rykova & Oke, 2015), the interaction of eddies with other eddies (Cresswell & Legeckis, 1986), the mean flow (e.g., Mata et al., 2006; Nilsson & Cresswell, 1981), and the ocean bottom (e.g., Oke & Griffin, 2011), and the impact of eddies on productivity (e.g., Everett et al., 2012) and marine biota (e.g., Suthers et al., 2011 and references therein). However, only one study describes the vertical circulation within an eddy in the EAC region. Oke and Griffin (2011) investigate the properties of a cyclonic eddy interacting with the eastern Australian continental shelf break. They show upwelling where the eddy appears to interact with the shelf break, downwelling in the opposite part of the eddy, and a nutrient enrichment in the euphotic zone in the vicinity of the eddy. Whether this vertical velocity pattern is common for EAC cyclonic eddies, or even existent within EAC anticyclonic eddies, is still unknown. Understanding the vertical circulation within long-lived EAC anticyclonic eddies is particularly relevant. EAC anticyclonic eddies have been shown to impact several oceanic regions as they propagate southward, leave the Tasman Sea, and reach the Eastern Indian Ocean (Pilo et al., 2015). These eddies have been shown to entrap coastal water organisms (Baird et al., 2011; Tranter et al., 1982), and affect the distribution of marine species (Ling et al., 2009). In addition, the number and strength of EAC anticyclonic eddies is predicted to increase in future climate scenarios (Oliver et al., 2015).

The purpose of this paper is to investigate patterns in the vertical circulation within EAC anticyclonic eddies. Specifically, we focus on the cells of upward and downward motion caused by the perturbation of the geostrophic flow of these eddies. We refer to this perturbation as "eddy distortion"—the change of eddy shape over time. Here we aim to further understand the mechanisms through which vertical velocity and eddy distortion are connected, and to gain additional understanding of this complex eddy dynamics. To this end, we use the output of a global, eddy-resolving model.

In the next section, we describe the ocean model used in this study, the eddies investigated, and our analysis methods. In section 3, we show patterns of vertical velocity and eddy distortion in EAC anticyclonic eddies. In section 4, we discuss mechanisms that link the change in eddy shape and vertical velocity, followed by a discussion and conclusions in section 5.

2. Data and Methods

We investigate eddies using the Ocean Forecasting Australia Model, version 3 (OFAM; Oke et al., 2013). OFAM is a near-global eddy-resolving model with a horizontal resolution of 1/10° and 51 vertical levels. The

vertical grid z* has 5 m spacing near the surface, 10 m spacing at 200 m depth, 120 m spacing at 1,000 m depth, and coarser grid spacing below that (Figure 1e, dashed lines). In this study, we show many results in depths between 500 and 1,500 m, where the vertical spacing ranges from 60 to 150 m. The model is run for

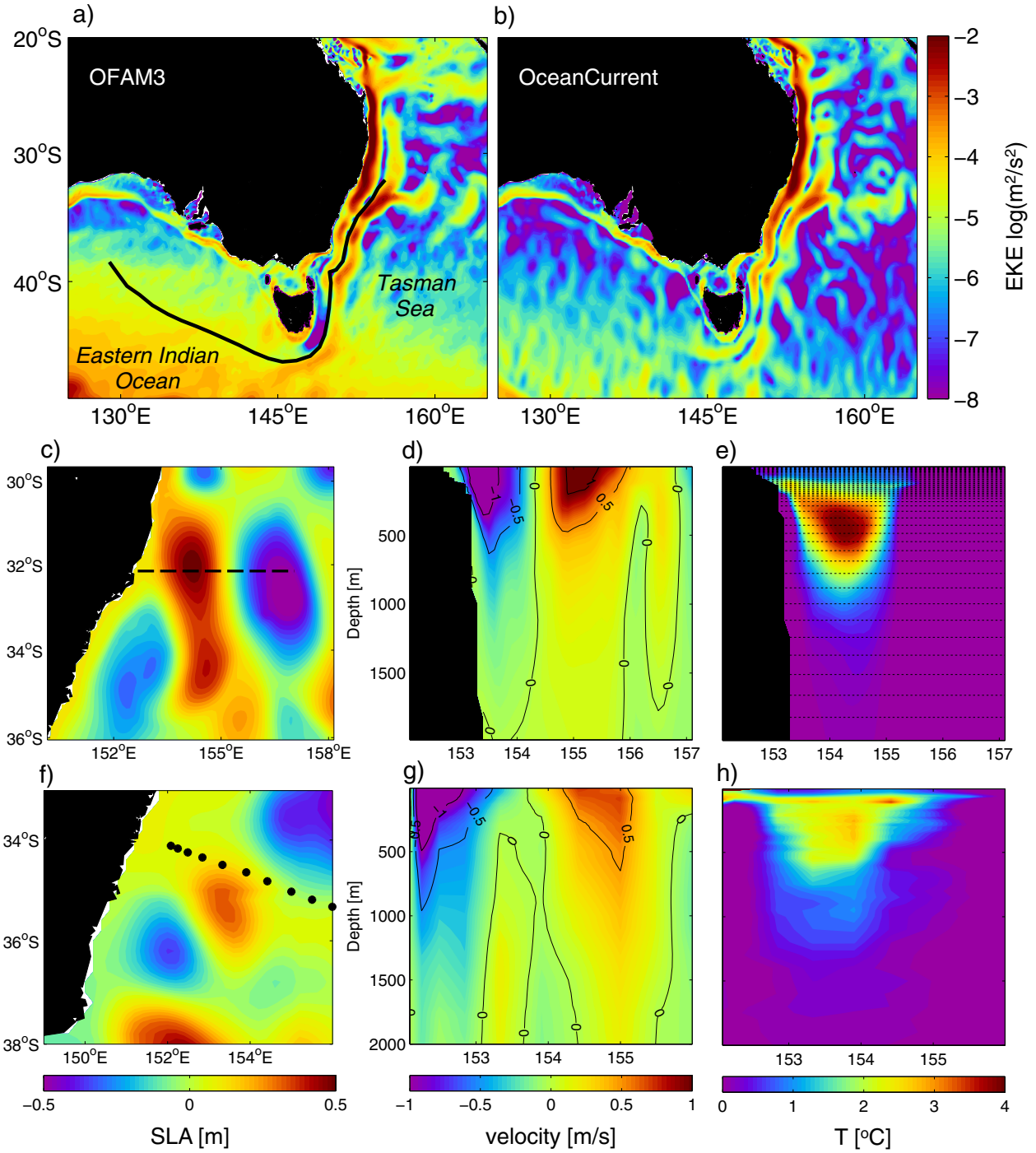

Figure 1. Comparison of the mean EKE between 2000 and 2005 from (a) OFAM and (b) OceanCurrent altimetry products (Deng et al., 2011); (c) SLA associated with an EAC anticyclonic eddy from the model; the dashed line indicates the location of the vertical section shown in (d) and (e); (d) modeled meridional velocity (colors and contours, spaced every 0.5 m/s) and (e) modeled temperature anomaly associated with the eddy shown in Figure 1c. The dotted vertical lines represent vertical levels of OFAM; (f) SLA from OceanCurrent altimetry products associated with a sampled EAC anticyclonic eddy (adapted from Ridgway et al., 2008); the black dots indicate CTD sampling stations; (g) geostrophic current relative to 2,000 dB computed from temperature and salinity fields (colors and contours, spaced every 0.5 m/s); (h) observed temperature, with CARS climatology (Ridgway & Dunn, 2003) removed.

36 years, with an 18 year spin-up, and forced with 3-hourly surface heat, freshwater, and momentum fluxes from ERA-Interim (Dee & Uppala, 2009), with restoring to monthly sea surface temperature (Reynolds et al., 2007, 10 day *e*-folding time scale); weak restoring to surface climatological salinity (Ridgway & Dunn, 2003, 180 day *e*-folding); and weak restoring to climatological temperature and salinity below 2,000 m depth (restoring time scale of 180 days). Because of the climatological restoring at depth and coarse vertical resolution, we only consider the top 2,000 m of the model fields throughout the manuscript.

We validate both horizontal and vertical representations of the eddy field in the model. First, we compare the mean eddy kinetic energy (EKE) between the model and a 1/4° resolution gridded altimetry product from OceanCurrent (Deng et al., 2011). Then, we compare vertical sections of geostrophic velocity and temperature anomaly between a modeled and an observed eddy.

The model realistically reproduces both the location and strength of the high EKE region off the east Australian continental shelf (Figures 1a and 1b). This high EKE region is associated with the meandering EAC and its eddies—both cyclonic and anticyclonic—, extending from where the EAC separates from the continental shelf break (~32°S) to the east of Tasmania (~42°S). Despite localised differences between the model and observations, the modeled regional circulation and variability are well represented.

The observed eddy used for comparison was sampled in May 2001 in full depth CTD casts (Ridgway et al., 2008, Figures 1f–1h). It is not mandatory for the dates of the observed eddy and the modeled eddy to be the same, as OFAM is a free-running model. Eddies from the EAC, however, display seasonal changes (Rykova & Oke, 2015). Therefore, it is important to compare eddies occurring in the region in the same season. The modeled eddy in Figures 1c–1e dates from May 1996. Despite being stronger than the sampled eddy (i.e., higher SLA, geostrophic velocity, and temperature anomaly), the dynamics and vertical structure of the modeled eddy are realistic. In both eddies, the geostrophic velocity (Figures 1d and 1g) and temperature (Figures 1e and 1h) signals penetrate below 1,000 m, with maximum temperature anomaly between ~200 and 600 m. We regard the model output to be suitable for investigating the dynamics of eddies from the EAC, consistent with previous studies (Oke & Griffin, 2011; Pilo et al., 2015; Rykova & Oke, 2015).

We analyze the vertical velocity in ten anticyclonic eddies that originate where the EAC separates from the continental shelf break (~31°S). We track the selected eddy by locating closed 0.1 m sea level anomaly (SLA) contours in weekly SLA fields, between 1993 and 2012. An eddy is continuous in time if it is evident at consecutive weeks, with a tolerance of 3 weeks. We track each eddy until the SLA associated with it becomes smaller than 0.1 m, or until it can no longer be identified as a closed contour feature. The tracking method, pathway, and evolution of these eddies are described in Pilo et al. (2015). After formation at the EAC separation region, the eddies propagate southward adjacent to the shelf break, cross south of Tasmania, and then advect westward toward the Eastern Indian Ocean (Figure 1a, black line). As they move along this pathway, eddies generally become deeper and more barotropic (Pilo et al., 2015).

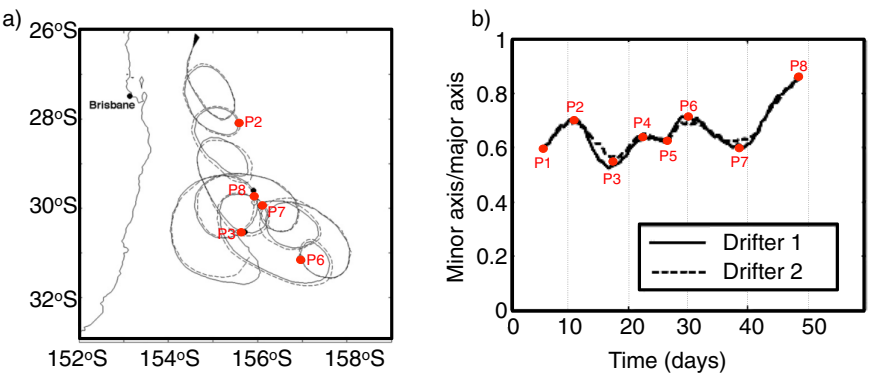

Figure 2. (a) Position of two surface drifters trapped in an anticyclonic eddy in the Tasman Sea between 21 February and 22 April 2007. Red points indicate the averaged location of the drifters 10, 20, 30, 40, and 50 days after their launch. (b) Time series of the ratio between the minor and the major axes of ellipses fitted to the trajectories shown in Figure 2a. Inflections on ratio curves are indicated by red points (P1–P8; adapted from Brassington, 2010).

For some of the analyses in this paper, we separate the eddy pathway according to the main direction of eddy propagation: southward and westward. As eddies propagate southward (i.e., between the EAC separation and off east Tasmania), they interact with bathymetry, with other eddies, and with a strong mean flow. In this part of the pathway, the vertical velocity can be induced by several mechanisms. As eddies propagate westward (i.e., off west Tasmania and the Eastern Indian Ocean), they are isolated, and the surrounding flow is quasi-quiescent. In this part of the pathway, eddies are more likely to behave as isolated case studies, and the vertical velocity induced by eddy distortion and eddy propagation to have clearer signals. In addition, as eddies propagate south

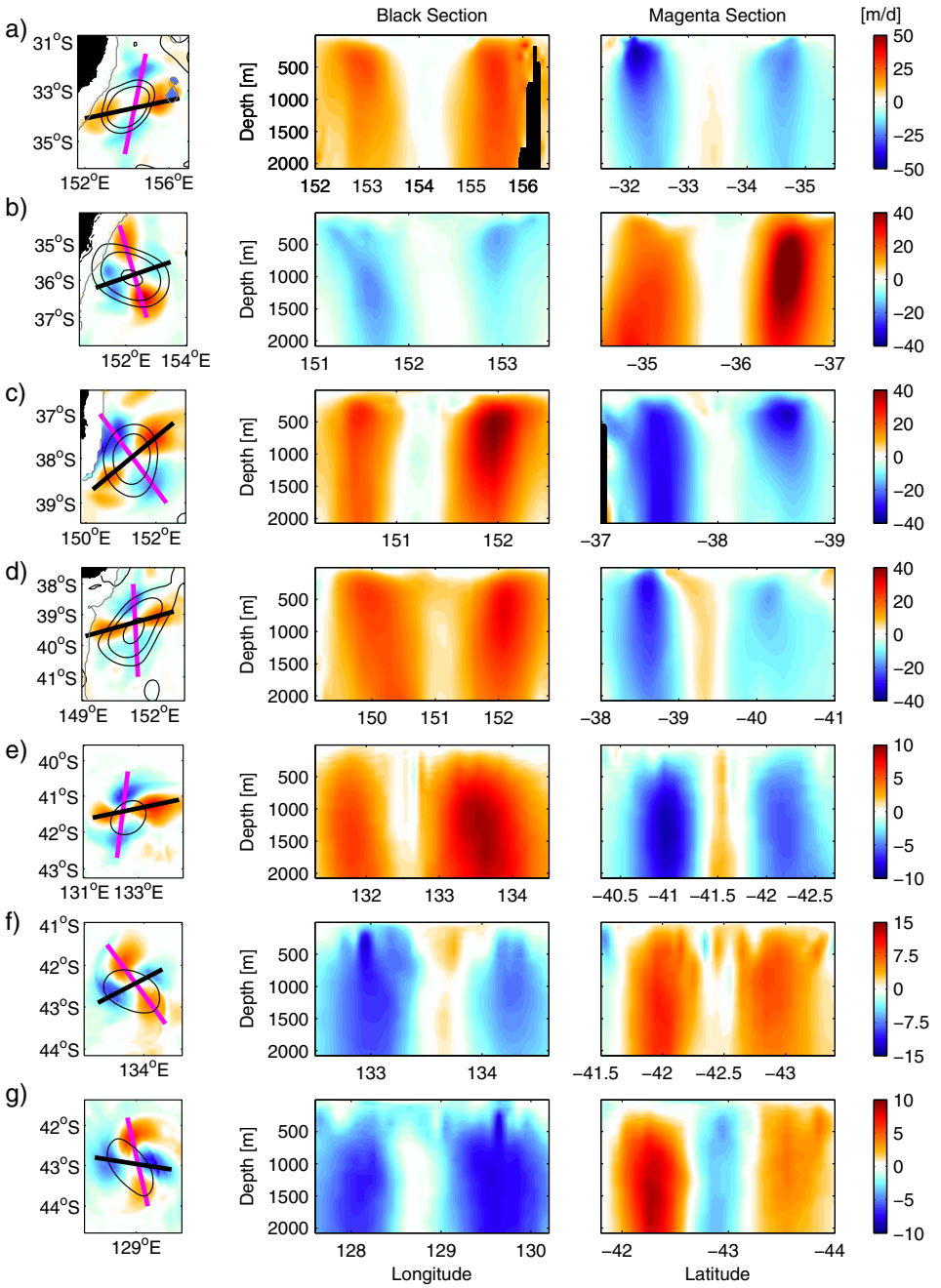

Figure 3. (left) Depth-averaged (0–2,000 m) vertical velocity (colors) in (a–g) seven EAC anticyclonic eddies from a near-global, eddy-resolving ocean model. Black lines indicate 0.1, 0.25, and 0.5 m sea level anomaly contours. Grey lines indicate the 3,000 m isobath. (right) The bold black (magenta) line indicates the location of the vertical section shown in the center. Note the different scales of vertical velocity for each eddy.

of Tasmania, between 146°E and 150°E, they become highly incoherent, shed a lot of filaments, and interact with seamounts and oceanic rises. Hence, the region south of Tasmania is not included in our analyses.

The vertical velocity is the least reliable variable in any ocean model, including the model used in this study. We perform an Empirical Orthogonal Function (EOF) analysis to eliminate the noise and to isolate the

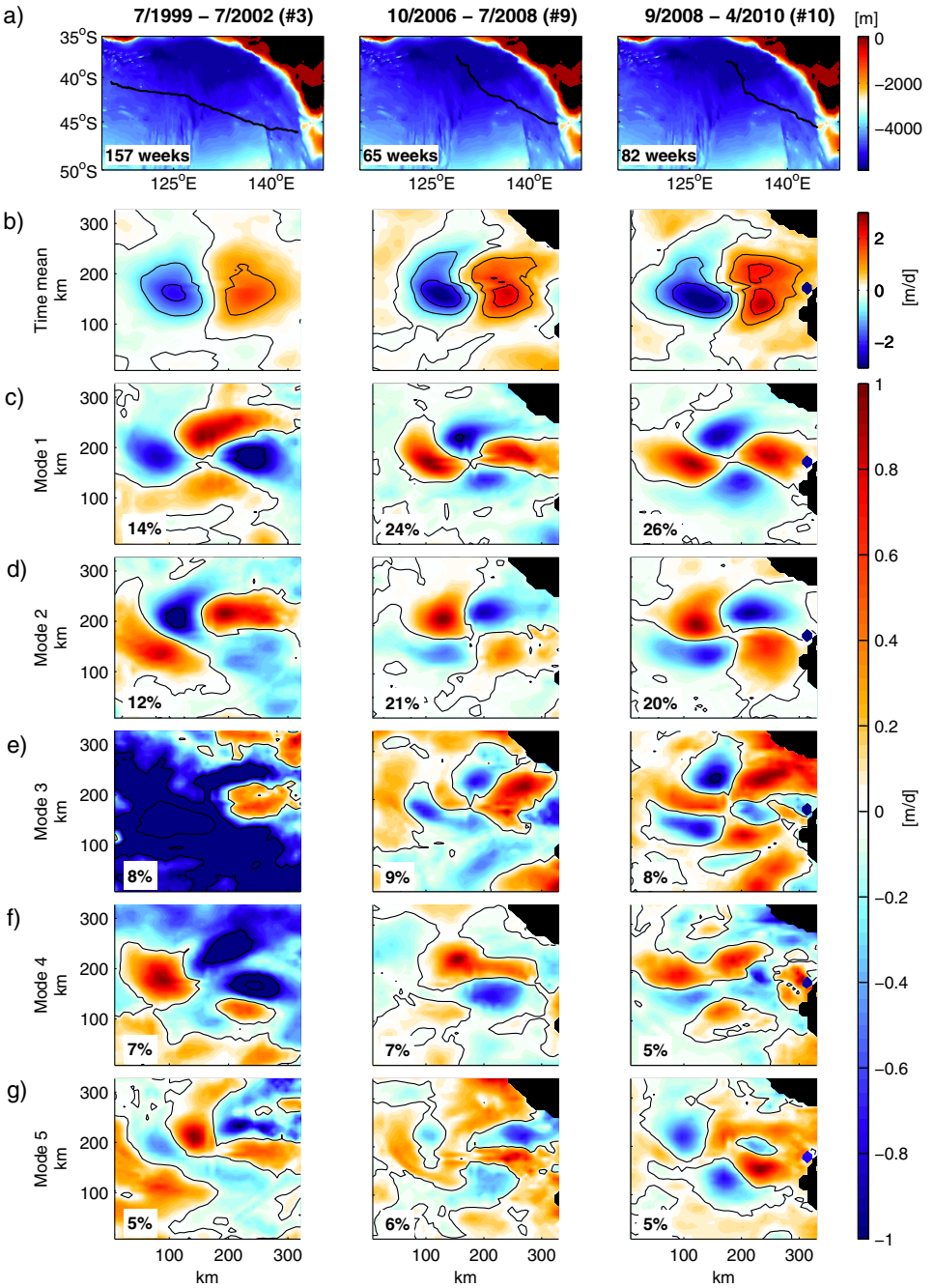

Figure 4. (a) Maps indicating the tracks (black lines) of three anticyclonic eddies propagating in the Eastern Indian Ocean. Colors denote bathymetry, and the numbers in the bottom left corners indicate the number of weeks taken for each eddy to propagate along the tracks. The numbers of the eddies (i.e., #3, #9, and #10) relate to Table 1. (b) Time mean depth-averaged (0–2,000 m) vertical velocity ($\tilde{w}$) for each eddy as they propagate along the tracks shown in Figure 4a. (c–g) EOF modes 1–5 of an EOF analysis of $\tilde{w}$, normalized by the maximum value of each mode, for each eddy. Black lines denote null $\tilde{w}$. The percentages in the bottom left corner are the amount of variance contained in each mode, for each eddy.

Table 1
Results From a Single-Variable EOF Analysis of Depth-Averaged Vertical Velocity ($\tilde{w}$) and From a Multivariate EOF Analysis of $\tilde{w}$ and Change in Sea Level Anomaly (ΔSLA) for 10 Anticyclonic Eddies

	Southward $\tilde{w}$		Westward $\tilde{w}$		Southward combined $\tilde{w}$ and ΔSLA		Westward combined $\tilde{w}$ and ΔSLA	
	EOF modes	Combined variance (%)	EOF modes	Combined variance (%)	EOF modes	Combined variance (%)	EOF modes	Combined variance (%)
#1	1, 2, 5	45	1–3	49	1–4	51	1–3	37
#2	1, 2, 4, 6, 7	52	1–4, 6	56	1, 3, 6	32	2, 3, 6,7	19
#3			1, 2, 6	31			2, 3	10
#4			1–6	50			1–5	57
#5	1, 2, 6, 7	47	1, 2	25	1, 2	38	2–4	15
#6	1, 2	38	1, 2, 4	46	1, 2	33	2, 3	19
#7	1, 9	22	1–3	38	1	19	2–4	26
#8	1, 2	37	1, 2, 4	48	1, 2, 6	34	2, 3	18
#9			1, 2	45			1–3	53
#10			1–3	54			1–3, 5	58

Note. The modes and the combined variances shown relate to the alternating cells of positive and negative values seen in Figures 4 and 6. The propagation of the 10 eddies is divided into two sections: southward, between the EAC separation region and east of Tasmania, and westward, in the Eastern Indian Ocean. Absent values in the southward section are due to the presence of shallow regions along the eddy path that hinder the results from the EOF analysis.

coherent components of the vertical velocity fields. The patterns of vertical velocity shown here are coherent, as we show in section 3.1. For the EOF analysis we use 4° × 4° maps of depth-averaged vertical velocity ($\tilde{w}$) for each time step of the eddy lifetime. First, we detrend the variable in time. Then, we compute a singular value decomposition of the anomaly field. The depths considered for the EOF analysis range from 0 to 600 m when eddies propagate southward and from 0 to 2,000 m when eddies propagate westward. This difference is because southward-propagating eddies move through shallower regions and extend to shallower depths than the westward-propagating eddies (Pilo et al., 2015).

We also perform a multivariate EOF analysis combining $\tilde{w}$ and changes in SLA (ΔSLA). ΔSLA is calculated by subtracting the SLA field in the first time step from the SLA field in the second time step, with weekly time

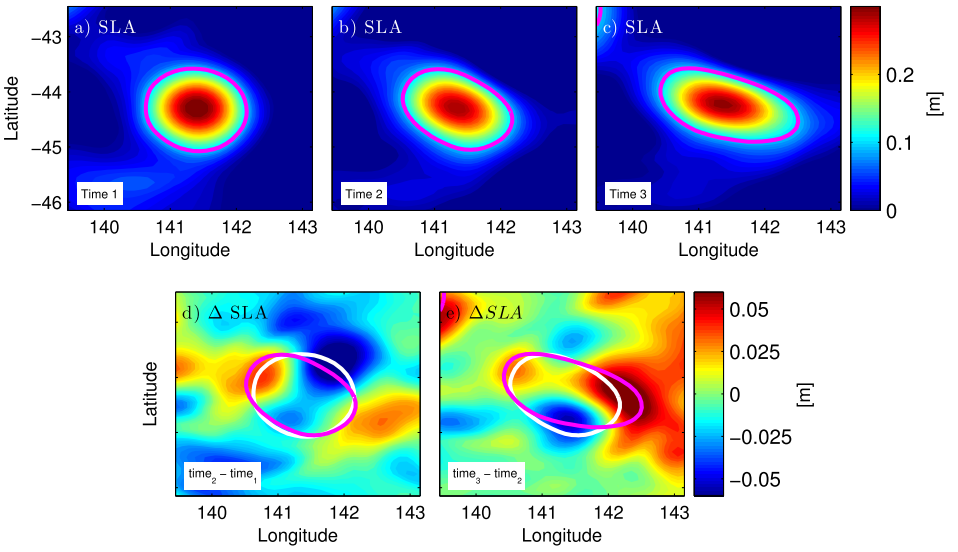

Figure 5. (a–c) Sea level anomaly (SLA) associated with one anticyclonic eddy at three subsequent weeks (times 1–3). The magenta line denotes the 0.1 m SLA contour; (d) change in SLA (ΔSLA) between times 2 (shown in Figure 5b) and 1 (shown in Figure 5a). The magenta line denotes the 0.1 m SLA contour in time 2, and the white line denotes the 0.1 m SLA contour in time 1; (e) as in Figure 5d, but for times 3 (shown in Figure 5c) and 2 (shown in Figure 5b).

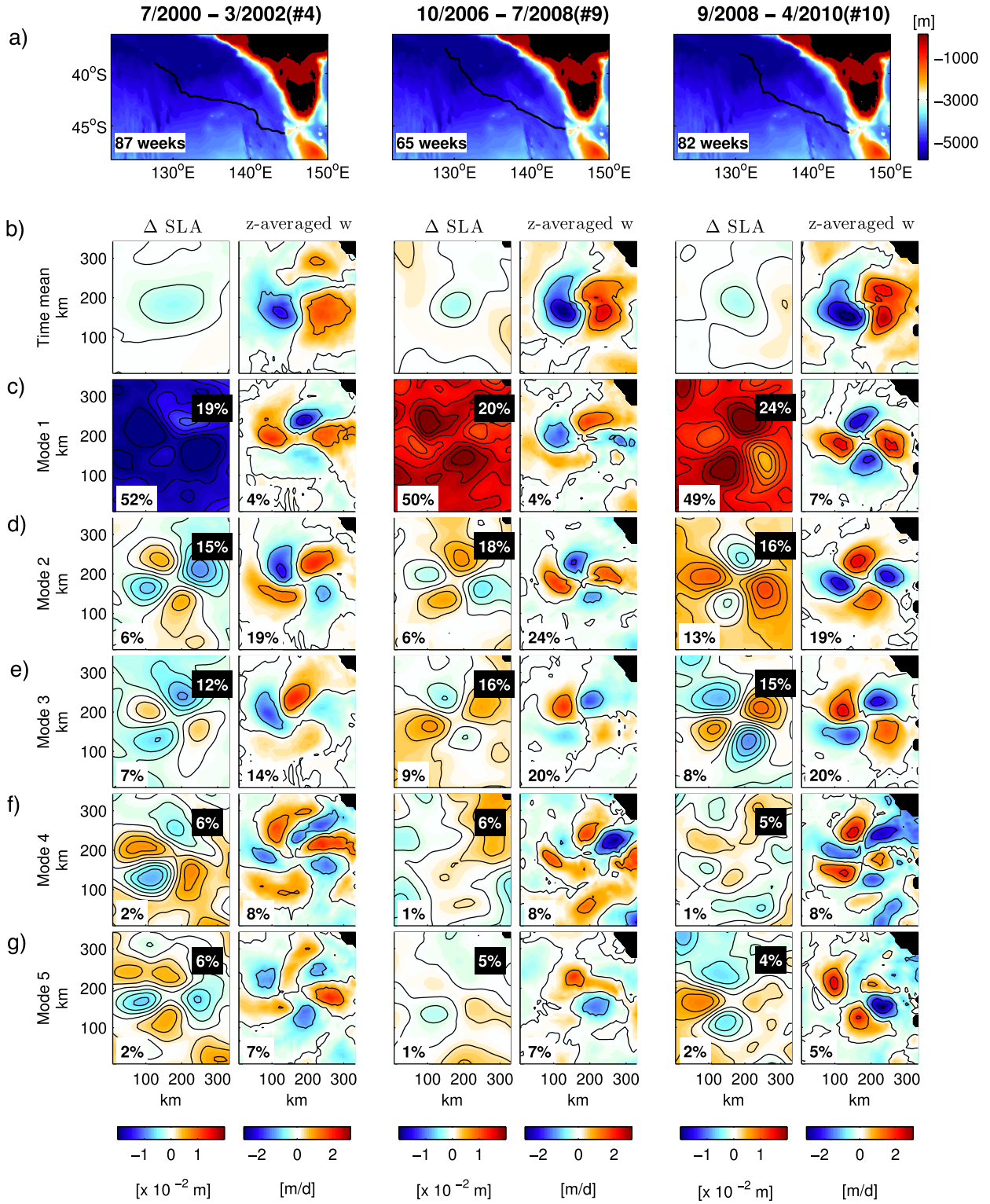

Figure 6. (a) Maps indicating the tracks of three anticyclonic eddies propagating in the Eastern Indian Ocean (black lines). Colors denote bathymetry, and the numbers in the bottom left corners indicate the number of weeks taken for each eddy to propagate along the tracks. The numbers of the eddies (i.e., #4, #9, and #10) relate to Table 1. (b) Time mean change in SLA (ΔSLA) and time mean depth-averaged (0–2,000 m) vertical velocity ($\tilde{w}$) for each eddy as they propagate along the tracks shown in Figure 6a. (c–g) EOF modes 1–5 of the multivariate EOF analysis of ΔSLA and $\tilde{w}$, normalized by the maximum value of each mode and then multiplied by each variable standard deviation, for each eddy (see section 3.3). Black lines denote null values. Percentages in white (black) boxes are the amount of variance contained in each mode for each variable (combined variable).

steps. These fields are aligned relative to the eddy center (maximum SLA). We then compare this weekly ΔSLA with the $\tilde{w}$ field in the second time step. For the multivariate EOFs, we normalize the variables by dividing each by their standard deviation, and build a combined matrix. We then detrend this combined matrix in time and perform the EOF analysis of the anomaly field. We calculate the variance of individual variables for each mode by dividing the EOF mode variance of a single variable by the variance of this variable's original signal.

Besides the 7 day interval used in the EOF analyses described above, we also test a shorter (e.g., 3 days) and a longer (e.g., 30 days) time interval. For a shorter interval the $\tilde{w}$ cells are absent, and for a longer interval the $\tilde{w}$ cells are present—but are less clear than in a 7 day interval. The results from this sensitivity test suggest that the eddy distorts—and hence impacts $\tilde{w}$—on a time interval between 3 and 30 days, and close to a time interval of 7 days. These results are supported by the findings of Brassington (2010), who shows the ratio between the minor and the major axes of ellipses fitted to the trajectory of two surface drifters trapped in an anticyclonic eddy in the Tasman Sea (Figure 2). This ratio—another proxy for eddy distortion—changes every ~5–10 days, to a large extent (i.e., between the red points in Figure 2b). This means that, on time intervals shorter than ~5–10 days, the eddy does not distort, and in time intervals longer than ~5–10 days the eddy distorts more than once. For example, between P2 and P7 (30 days apart), the ratio between the minor and the major axes of the ellipses is reduced by 14% (i.e., the eddy becomes more isotropic). However, the ratio changes five times over these 30 days, and the eddy becomes more or less isotropic each time. The change between P2 and P7, therefore, is an unrealistic assessment of eddy distortion. In the same way, an EOF analysis considering ΔSLA with a 30 day interval would also be unrealistic. Considering the results from the sensitivity tests and the findings by Brassington (2010), we determine the weekly time interval to be appropriate for the analyses performed here. This time interval seems to correspond to the time scale on which EAC eddies typically distort, or change shape. However, this time scale might be dependent on the interactions of the eddy with the mean flow, the wind, the ocean floor, and with other eddies.

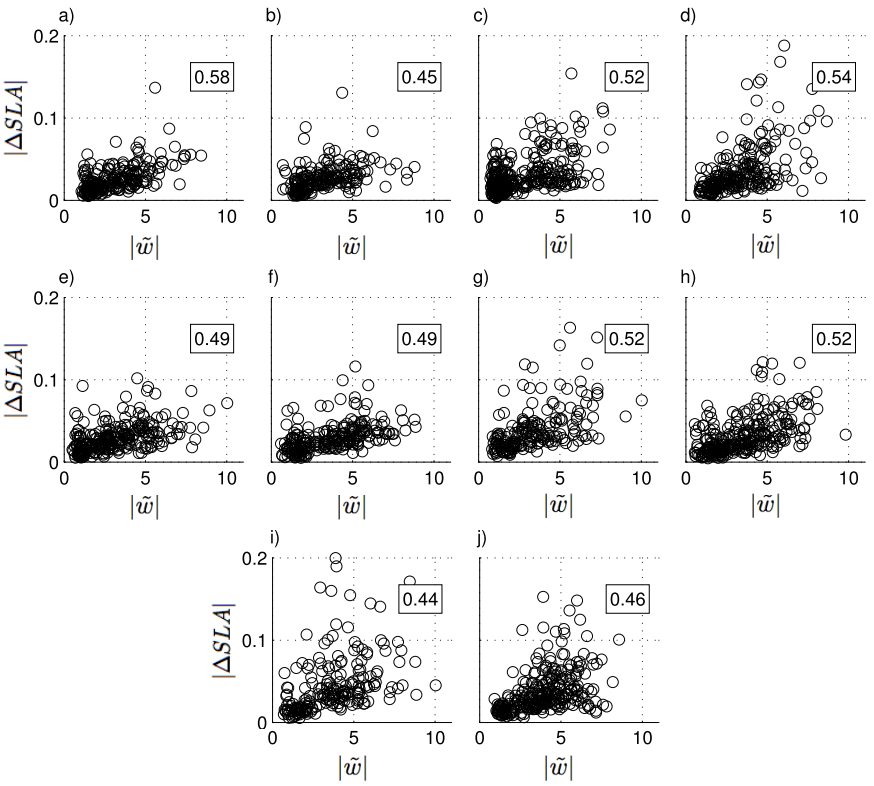

Figure 7. Values of absolute depth-averaged vertical velocity ($|\tilde{w}|$) and absolute change in sea level anomaly ($|\Delta SLA|$) (a–j) for 10 anticyclonic eddies for all time steps of their propagation between the EAC separation region to the Eastern Indian Ocean. The numbers in the boxes denote the correlation coefficient between these values.

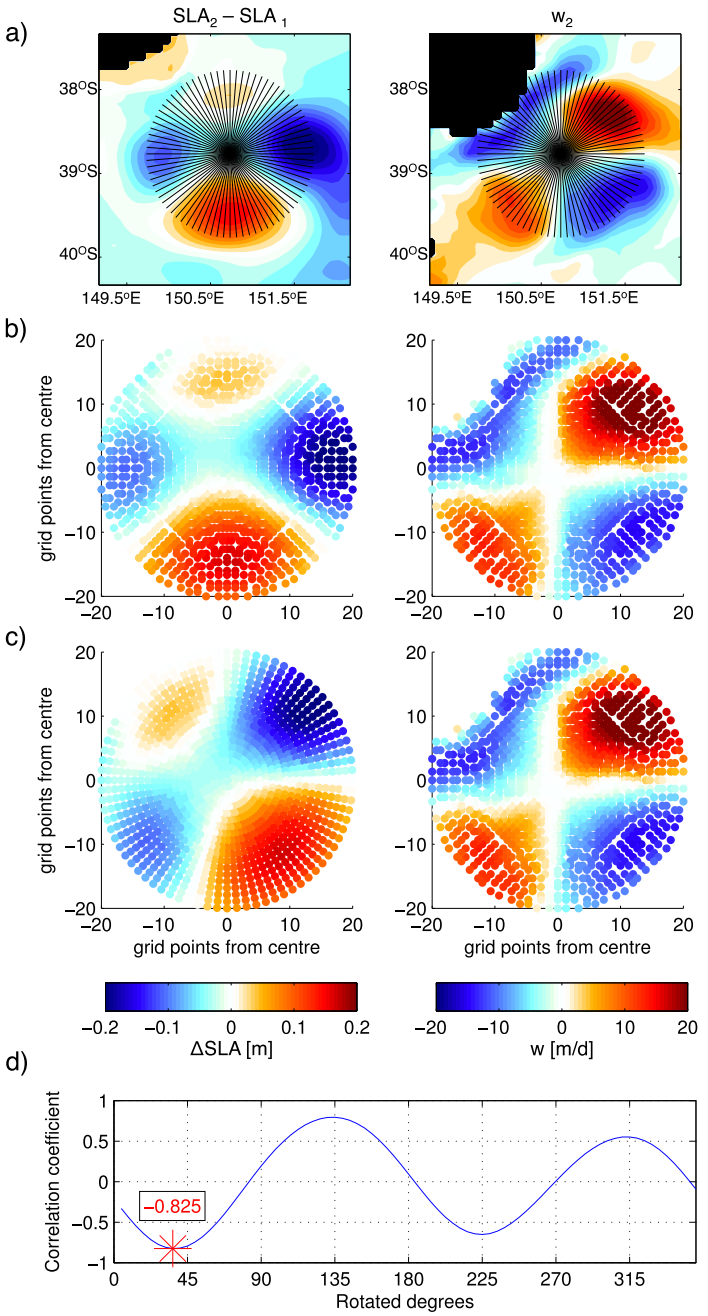

Figure 8. (a) (left) ΔSLA and (right) $\tilde{w}$ (colors) fields associated with an anticyclonic eddy located off Bass Strait. The black lines indicate the grid onto which these fields will be regridded; (b) as in Figure 8a, but with values in a radial grid; (c) as in Figure 8b, but with (left) ΔSLA rotated 31.5° anticlockwise, to match (right) $\tilde{w}$; (d) two-dimensional correlation coefficient between ΔSLA and $\tilde{w}$ from Figure 8b, considering different rotation angles for (left) ΔSLA (Figure 8b). The star indicates the correlation coefficient between the rotated ΔSLA and the nonrotated $\tilde{w}$ shown in Figure 8c.

3. Results

3.1. Eddy Vertical Velocity

The $\tilde{w}$ (surface to 2,000 m) in anticyclonic eddies formed at the EAC has alternating upward and downward cells (Figure 3, first column). These cells are stronger at depth (500–1,500 m), in most cases do not reach the surface, and are, sometimes, asymmetric (Figure 3; second and third columns). As eddies propagate, $\tilde{w}$ cells rotate in the same direction as the eddy rotation (i.e., anticlockwise). The existence of these $\tilde{w}$ cells indicates that the eddies are not in geostrophic balance and are, therefore, ageostrophic.

This pattern of alternating cells is seen along the whole eddy pathway (black line in Figure 1a). As eddies propagate southward, they are relatively strong (maximum SLA $>$ 0.5 cm) and have strong vertical velocity (up to 50 m/d in magnitude; Figures 3a–3d). Conversely, as eddies propagate westward, they are relatively weak (maximum SLA $<$ 0.2 cm) and have weaker vertical velocity (up to 15 m/d in magnitude; Figures 3e–3g).

We expect the pattern of alternating cells to be clearer and easier to observe in westward-propagating eddies than in southward-propagating eddies, owing to the quiescent aspect of the Eastern Indian Ocean. However, in both sections of the pathway, the pattern is clear and explains 22–56% of the combined variance of $\tilde{w}$ (Figure 4 and Table 1). This high variance is present regardless of the interactions between the eddy, the mean flow, the ocean bottom, and other eddies. Here we consider the combined variance of different EOF modes because the pattern of alternating cells rotates in time, appearing in up to six modes in the simple EOF analysis. In eddy #10, for example, the alternating $\tilde{w}$ cells are seen in modes 1–3 (Figure 4, third column). Despite this pattern distribution in different EOF modes, the results show that the alternating upward and downward cells are coherent in eddies that are either isolated or interacting with the surrounding environment.

3.2. Eddy Distortion

The isotropy of an eddy changes as it propagates in the ocean (e.g., Brassington, 2010; Cushman-Roisin et al., 1985). We refer to these changes in eddy isotropy as eddy distortion. Several factors are likely to contribute to eddy distortion, including interactions with bathymetry, with the mean flow, and with other mesoscale features. An example of eddy distortion is shown in Figure 5, with a semiisotropic eddy (Figure 5a) distorting in the northwest-southeast direction (Figures 5b and 5c) for 2 weeks. The ΔSLA field, obtained by subtracting SLA fields between subsequent weeks, shows alternating cells of positive and negative ΔSLA (Figures 5d and 5e). A positive cell indicates that the eddy distorted *toward* this area, and a negative cell indicates that the eddy distorted *away* from this area, relative to the previous week.

We considered rotating the SLA field in the first time interval before calculating ΔSLA. This approach would isolate changes associated with eddy distortion from changes associated with eddy rotation. We would have to assume, however, that eddies rotate as a solid body. This is not true, and we could not determine a rotation value appropriate for the analysis. We tested different rotation values for the SLA field in the first time interval and all the ΔSLA calculated exhibited alternating cells (see supporting information). For all rotation values, the cells had similar intensity, but different spatial distribution. With these results in

mind, we chose not to rotate the eddy in the first time interval and to know that the associated error is qualitative, and not quantitative.

3.3. Eddy Vertical Velocity and Distortion

Patterns of both $\tilde{w}$ and ΔSLA have alternating cells of positive and negative values. A multivariate EOF analysis, combining these variables, shows that $\tilde{w}$ and ΔSLA vary together (Figure 6) and explain 18–51% of the combined variance (Table 1). Again, we consider the combined variance of different EOF modes because the patterns of both variables rotate in time, appearing in several EOF modes (Figure 6).

Figure 6 shows three case studies of eddies propagating westward in the Eastern Indian Ocean. In these eddies, the pattern of alternating cells for both $\tilde{w}$ and ΔSLA is seen in the first three modes of variance (Figures 6c–6e). The $\tilde{w}$ cells are shifted anticlockwise in relation to the ΔSLA cells (e.g., Figure 6d, first and second plots). This shift is due to the nonrotation of the SLA field in the first time interval (see section 3.2 and supporting information), and because we compare a change in time (ΔSLA) to an instant field ($\tilde{w}$). If these were Southern Hemisphere cyclonic eddies, the $\tilde{w}$ cells would be shifted clockwise in relation to the ΔSLA cells. Despite the anticlockwise shift, all ΔSLA and $\tilde{w}$ pairs agree, and are inversely related (i.e., the cells of one variable are positive at the same time the cells of the other variable are negative). This means that an outward distortion (positive ΔSLA) is associated with downward motion (negative $\tilde{w}$), and an inward distortion (negative ΔSLA) is associated with upward motion (positive $\tilde{w}$).

To further show the relationship between ΔSLA and $\tilde{w}$ within eddies, we calculate the correlation between these variables (Figure 7). First, we isolate the values of absolute ΔSLA and absolute $\tilde{w}$ within a circle of 140 km radius centered in the eddy center (i.e., maximum SLA). Second, we calculate the spatial mean of these values. This process is repeated at each time interval as the eddy propagates. Therefore, the variables that are correlated at each time interval are the mean absolute $|\Delta SLA|$ and the mean absolute $|\tilde{w}|$ within the eddy. The rationale for relating these variables is that the stronger the eddy distortion (i.e., the higher the values of $|\Delta SLA|$), the stronger the vertical circulation within the eddy.

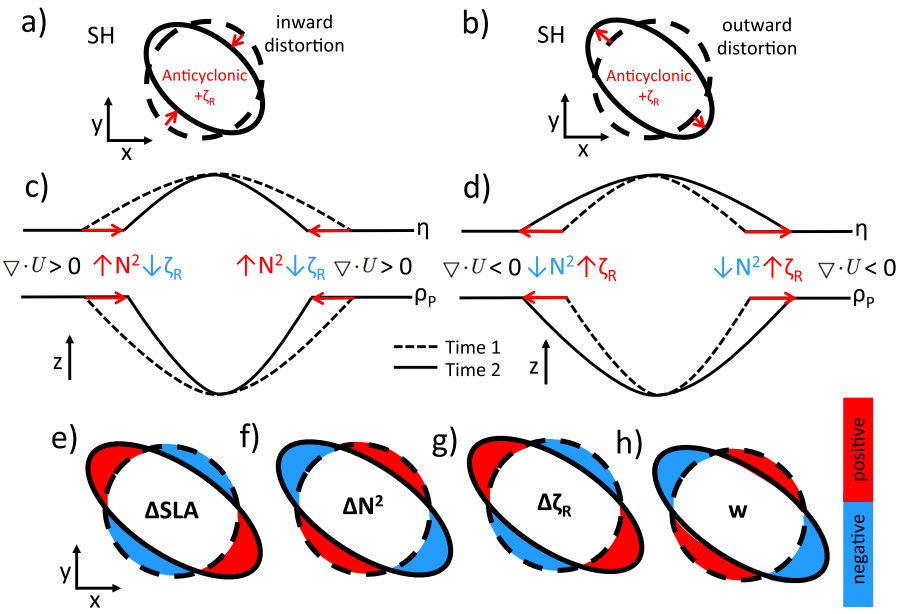

Figure 9. Schematics of a Southern Hemisphere (SH) anticyclonic eddy distorting (a) inward and (b) outward; changes in stratification (N^2) and in relative vorticity (ζ_R) in the eddy interior associated with an (c) inward and (d) outward distortion shown in. η is the ocean's free surface and ρ_P is the isopycnal at the bottom of the permanent pycnocline. (e) Changes in SLA (ΔSLA), (f) stratification (ΔN^2), and (g) relative vorticity ($\Delta\zeta_R$) between subsequent time steps associated with eddy distortion. The vertical velocity pattern in the final time step associated with these distortions is shown in (h). From Figures 9a–9h, the dashed black lines indicate the eddy shape before distortion, and the solid black line indicates the eddy shape after distortion.

For the ten anticyclonic eddies analyzed in this study, the correlation between $|\Delta SLA|$ and $|\tilde{w}|$ ranges from 0.44 to 0.58 (Figure 7). Note that this correlation is always positive because we compare absolute values of ΔSLA and $\tilde{w}$. Also note that the values within the 140 km-radius circle established here mostly include waters from the eddy interior, but there is some contribution from waters from the surrounding ocean. Despite the relatively low correlation values in Figure 7, the results indicate that there is some correlation between $|\Delta SLA|$ and $|\tilde{w}|$.

Another way to correlate the ΔSLA and the $\tilde{w}$ cells is by performing a two-dimensional correlation analysis. In this analysis, the ΔSLA at each point within the eddy is compared to the $\tilde{w}$ considering all depth layers below these points (remember that $\tilde{w}$ is the depth-averaged vertical velocity). However, because of the anticlockwise shift of $\tilde{w}$ cells in relation to the ΔSLA cells described above, the correlation coefficient resulting from this two-dimensional analysis is low. To eliminate this shift between the patterns, we rotate the ΔSLA fields anticlockwise, until they match the nonrotated $\tilde{w}$ fields.

Figure 8 shows an example of a two-dimensional correlation analysis for a particularly clear example. This analysis is done as follows. First, we regrid the ΔSLA and the $\tilde{w}$ fields onto a radial grid (Figure 8a). This grid has a ~160 km radius centered in the eddy center, and has a resolution of ~8.3 km × 4.5° (80 radial lines with 20 grid points per line; Figure 8d). We then rotate the regridded ΔSLA values one radial line (i.e., 4.5°) at a time, from zero to 360°. For each rotation we calculate the two-dimensional correlation coefficient (Figure 8d). As the ΔSLA rotates, the correlation coefficient oscillates between positive and negative values. Because we show in Figure 6 that ΔSLA and $\tilde{w}$ have an inverse relationship, we look for the first minimum correlation coefficient as we rotate ΔSLA anticlockwise (red star in Figure 8d). For the example shown in Figure 8, the correlation coefficient between the nonrotated ΔSLA pattern and the $\tilde{w}$ pattern is −0.33. After the ΔSLA pattern is rotated, this value increases to −0.82.

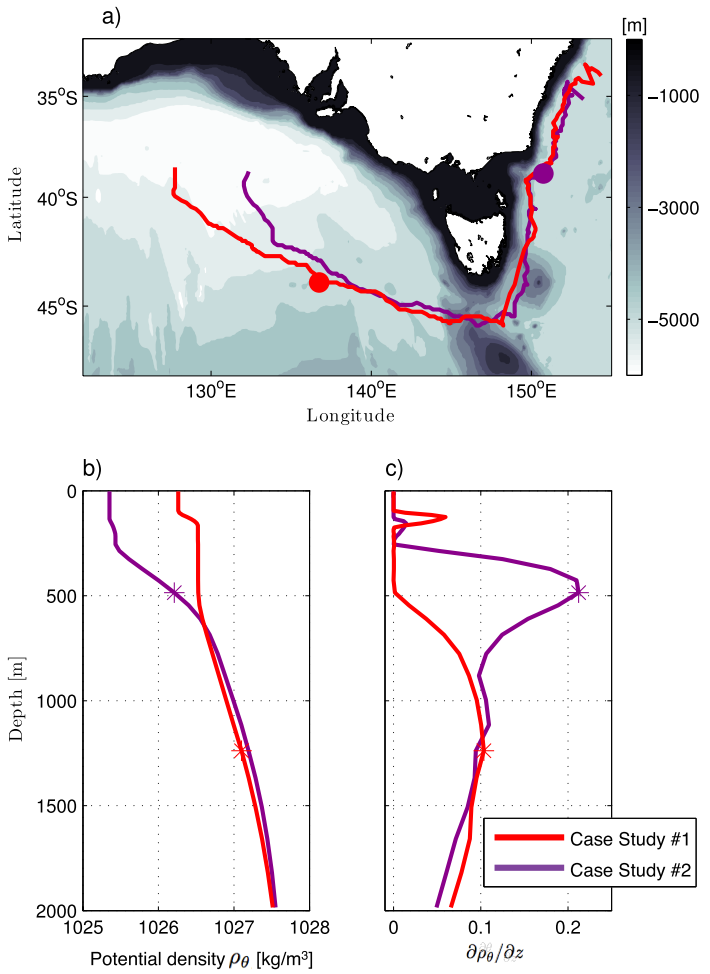

Figure 10. (a) Map indicating the tracks of two anticyclonic eddies chosen as case studies. The red lines relates to case study #1, with the selected location for the analysis shown here indicated by the red dot. The purple line and dot relate to case study #2. Grey colors denote bathymetry. (b) Vertical profile of potential density (ρ_θ) in the eddy center (i.e., below the maximum SLA) of case studies #1 (red) and #2 (purple). (c) As in Figure 10b, but for the change of potential density in depth ($\partial\rho_\theta/\partial z$). The stars in Figures 10b and 10c indicate the bottom of the permanent pycnocline.

4. Linking Eddy Distortion to Vertical Velocity

We now discuss two mechanisms that link eddy distortion to vertical velocity. One mechanism is based on the conservation of potential vorticity (Q) and the other, on the conservation of volume—relating to the convergence and divergence of the horizontal flow as the eddy distorts.

The first mechanism, based on conservation of potential vorticity (Q), focuses on the relationship between stratification and relative vorticity within the eddy. The isopycnic Ertel's potential vorticity Q (Ertel, 1940; Gill, 1982), considering the horizontal velocity components to be depth independent, is

$$Q=(f+\zeta_R)\frac{N^2}{g}, \tag{1}$$

where f is the Coriolis parameter, ζ_R is the vertical component of the relative vorticity ($\partial v/\partial x-\partial u/\partial y$), g is the acceleration of gravity, and N^2 is the Brunt-Väisälä frequency:

$$N^2=\frac{g}{\rho}\frac{\partial\rho}{\partial z}, \tag{2}$$

where ρ_{theta} is the potential density and z are depth levels.

Q relates stratification and ζ_R of a rotating fluid and is conserved in an adiabatic, frictionless motion. We assume Q to be conservative and f to be constant between time intervals. To conserve Q, a change in N^2

has a compensating change in ζ_R. In this manner, the conservation of Q connects the eddy distortion to the alternating cells of vertical velocity, and we explain the concept schematically in Figure 9. As an eddy distorts, it changes the SLA and the underlying stratification (N^2), as isopycnals move vertically (Figures 9a–9d). The change in SLA impacts the N^2 because, to a large extent, the sea surface height represents the integral properties of the water column below. As Q is conservative, when stratification changes, ζ_R also changes. A decrease in N^2 is compensated by a gain in positive ζ_R, which has anticyclonic rotation in the Southern Hemisphere. Conversely, an increase in N^2 is compensated by a gain in negative ζ_R, which has cyclonic rotation in the Southern Hemisphere. The changes in the sea level and in the eddy interior are seen as alternating cells of ΔSLA, ΔN^2 and $\Delta\zeta_R$ (Figures 9e–9g). Due to conservation of momentum and the rotation associated with the $\Delta\zeta_R$, upward and downward cells develop (Figure 9h). These interior changes in the eddy may explain the pattern of alternating cells seen in $\tilde{w}$.

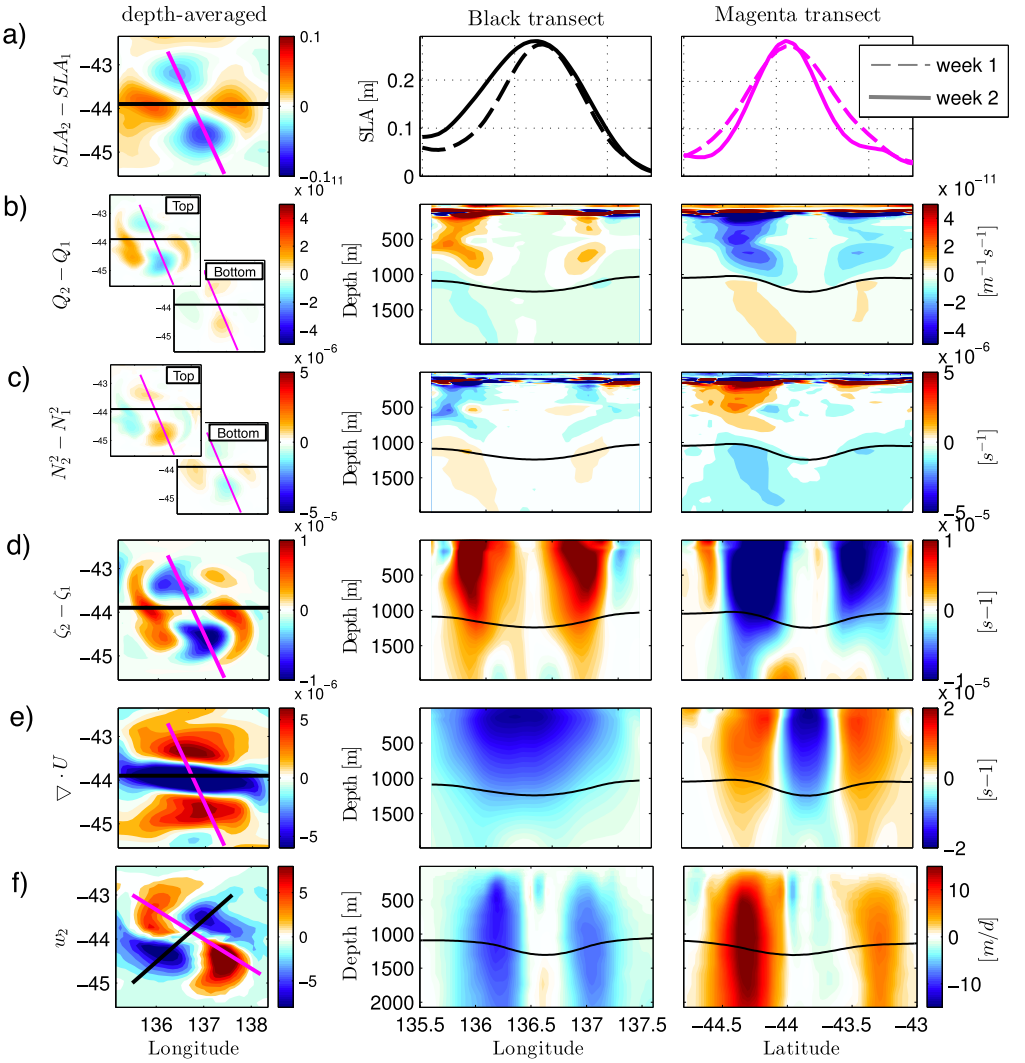

Figure 11. Change in (a) sea level anomaly (SLA), (b) depth-averaged potential vorticity (Q), (c) depth-averaged stratification (N^2), and (d) depth-averaged relative vorticity (ζ_R; colors, left) between subsequent time steps (t_1 and t_2) for an anticyclonic eddy in the Eastern Indian Ocean (i.e., case study #1). The black and the magenta lines denote the location of the vertical sections shown in the middle and in the right columns; depth-averaged (e) horizontal divergence ($\nabla \cdot U_2$) and (f) vertical velocity ($\tilde{w}$) in the final time step (colors, left). The top and bottom plots in Figures 11b and 11c show the depth-averaged variables above and below the permanent pycnocline. In Figures 11d–11f, the variables are averaged between 0 and 2,000 m. The black and the magenta lines in the left column denote the location of the vertical sections shown in the middle and in the right columns. The black lines in the middle and right columns from Figure 11b to 11f denote the isopycnal at the base of the permanent pycnocline (1,027.1 kg/m^3).

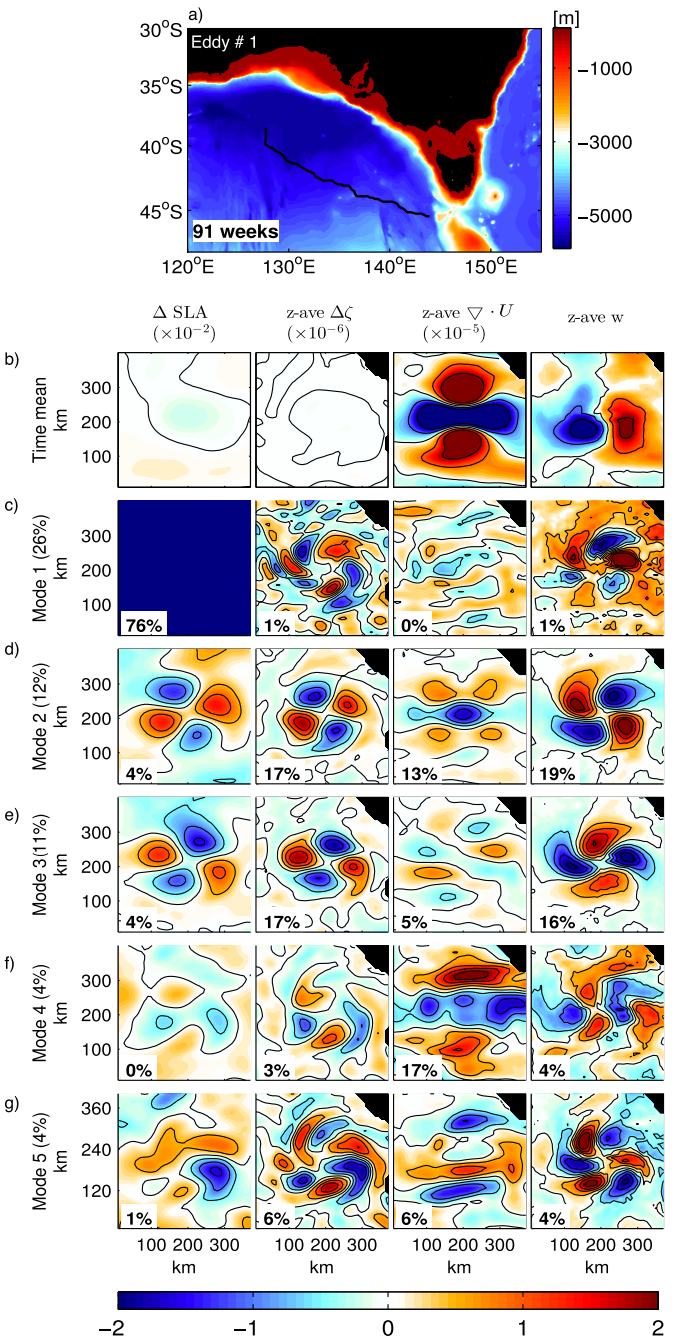

Figure 12. (a) Map indicating the track of an anticyclonic eddy (case study #1) propagating in the Eastern Indian Ocean (black line). Colors denote bathymetry, and the number in the bottom left corner indicate the number of weeks taken for this eddy to propagate along the track. (b) Time mean change in SLA (ΔSLA) and time mean depth-averaged (0–2,000 m) relative vorticity (ζ_R), horizontal divergence ($\nabla \cdot U_2$), and vertical velocity ($\tilde{w}$) for this eddy as it propagates along the track shown in Figure 12a. (c–g) EOF modes 1–5 of the multivariate EOF analysis of ΔSLA, (ζ_R), $\nabla \cdot U_2$, and $\tilde{w}$, normalized by the maximum value of each mode and then multiplied by each variable standard deviation, for each eddy (see section 3.3). Black lines denote null values. Percentages in white boxes are the amount of variance contained in each mode for each variable, and percentages in *y* axis label are the amount of variance for the combined variables.

The second mechanism, based on the conservation of volume, relies on the continuity within the eddy as it distorts. The eddies studied here are ageostrophic and, therefore, the divergence of their horizontal flow is nonzero. An inward distortion relates to divergence of the flow, inducing upward motion. Conversely, an outward distortion relates to convergence of the flow, inducing downward motion. This mechanism results in the same $\tilde{w}$ pattern as the mechanism proposed before.

4.1. Case Studies

We test these mechanisms considering two case studies of anticyclonic eddies, both originating in the EAC separation region. First, we show model fields at two locations along the trajectory of these eddies. Second, for a robust analysis, we calculate combined EOFs considering more time steps of the lifetime of these eddies.

For eddy #1, we investigate its structure when it is located in the Eastern Indian Ocean (Figure 10a, red dot). For eddy #2, we investigate its structure when it is located off Bass Strait (Figure 10a, purple dot). The structure of these eddies, in these different locations, differs in several ways. When eddy #1 is located in the Eastern Indian Ocean, it has a subsurface core, is relatively weak (0.3 m SLA and 0.4 m/s rotation speed), and is isolated from the bottom and from strong mean flow interactions. When eddy #2 is located off Bass Strait, it is surface intensified, relatively strong (0.5 m SLA and 1.2 m/s rotation speed), and interacts with the continental shelf break. Surface intensified eddies depress both the seasonal and the permanent pycnoclines. Conversely, eddies with a subsurface core have a thick layer of water that deepens the permanent pycnocline but shoals the seasonal pycnocline (e.g., mode water eddies; McGillicuddy, 2015). We define the permanent pycnocline as the maximum vertical density gradient that is not associated with the surface mixed layer. This pycnocline can be relatively shallow in surface intensified eddies (Figures 10b and 10c; purple lines) and relatively deep in eddies with a subsurface core (Figures 10b and 10c; red lines).

4.1.1. Eddy #1 in the Eastern Indian Ocean

When eddy #1 is located in the Eastern Indian Ocean, it has a mixed layer extending down to 500 m and a permanent pycnocline located at ~1,300 m (Figures 10b and 10c). The thick mixed layer results from the several warming and cooling seasons the eddy has encountered since its formation (Nilsson & Cresswell, 1981). At this location, 76% of the horizontal velocity of the eddy is projected onto the barotropic mode, and 18% is projected onto the first baroclinic mode (Pilo et al., 2015).

We calculate ΔQ, ΔN^2, and $\Delta \zeta_R$ considering subsequent time intervals, in the same manner as we calculate ΔSLA, described in section 2. Here we also choose not to rotate the eddy in the first time interval. In 1 week, this eddy distorts outward in longitude and inward in latitude (Figure 11a). Q and f are constant between the weeks analyzed ($\Delta Q \ll Q$ and $\Delta f \ll f$). Therefore, N^2 and ζ_R change together to conserve Q, and we can further assess how the eddy distortion relates to dynamical changes in the eddy interior.

As the eddy distorts inward, a region with previously high SLA now has lower SLA (Figure 11a, magenta section). This decrease in SLA

changes N^2 below (Figure 11c). Above (below) the permanent pycnocline, N^2 increases (decreases), as isopycnals previously depressed (compressed) relax back to their normal state. The ΔN^2 above the pycnocline is of order 10^{-6} s^{-1}, and below, of order 10^{-7} s^{-1}. This stronger ΔN^2 at the top is expected, as the response of isopycnals to sea level changes decreases in depth. The increase in N^2 occurring above the pycnocline is balanced by a gain in negative ζ_R, which is consistent in depth (Figure 11d). Negative ζ_R has cyclonic rotation in the Southern Hemisphere. A positive vertical velocity (i.e., upward motion) in the final week results from these dynamical changes (Figure 11f). The $\tilde{w}$ cells are shifted anticlockwise in relation to the other variables, as shown before in section 3.3. In addition, this inward distortion is associated with divergence of the horizontal flow (Figure 11e; magenta section). Therefore, we conclude that an inward distortion induces upward motion.

As the eddy distorts outward, a region with previously low SLA now have higher SLA, depressing isopycnals below (Figure 11a, black section). Therefore, the layers above the permanent pycnocline become less stratified, seen as a negative ΔN^2 (Figure 11c). A negative ΔN^2 above the permanent pycnocline is balanced by a positive $\Delta\zeta_R$ (Figure 11d). The positive ζ_R has anticyclonic rotation in the Southern Hemisphere, resulting in a negative vertical velocity (i.e., downward motion) in the final week (Figure 11f). In addition, this outward distortion is associated with convergence of the horizontal flow (Figure 11e; black section). Therefore, we conclude that an outward distortion induces downward motion.

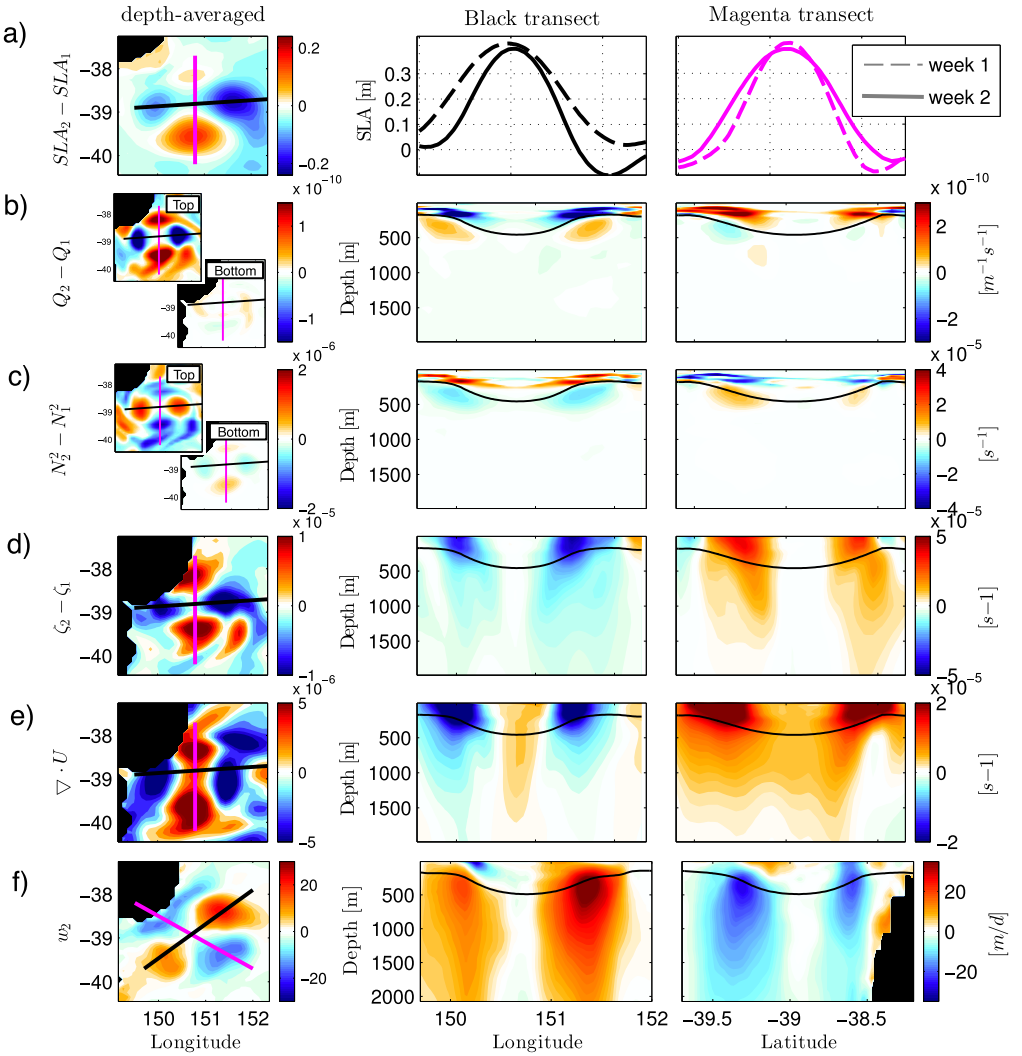

Figure 13. Same as in Figure 11, but for an anticyclonic eddy off Bass Strait (i.e., case study #2). The black lines in the middle and right columns from (b) to (f) denotes the isopycnal in the end of the permanent pycnocline (1,026.3 kg/m^3).

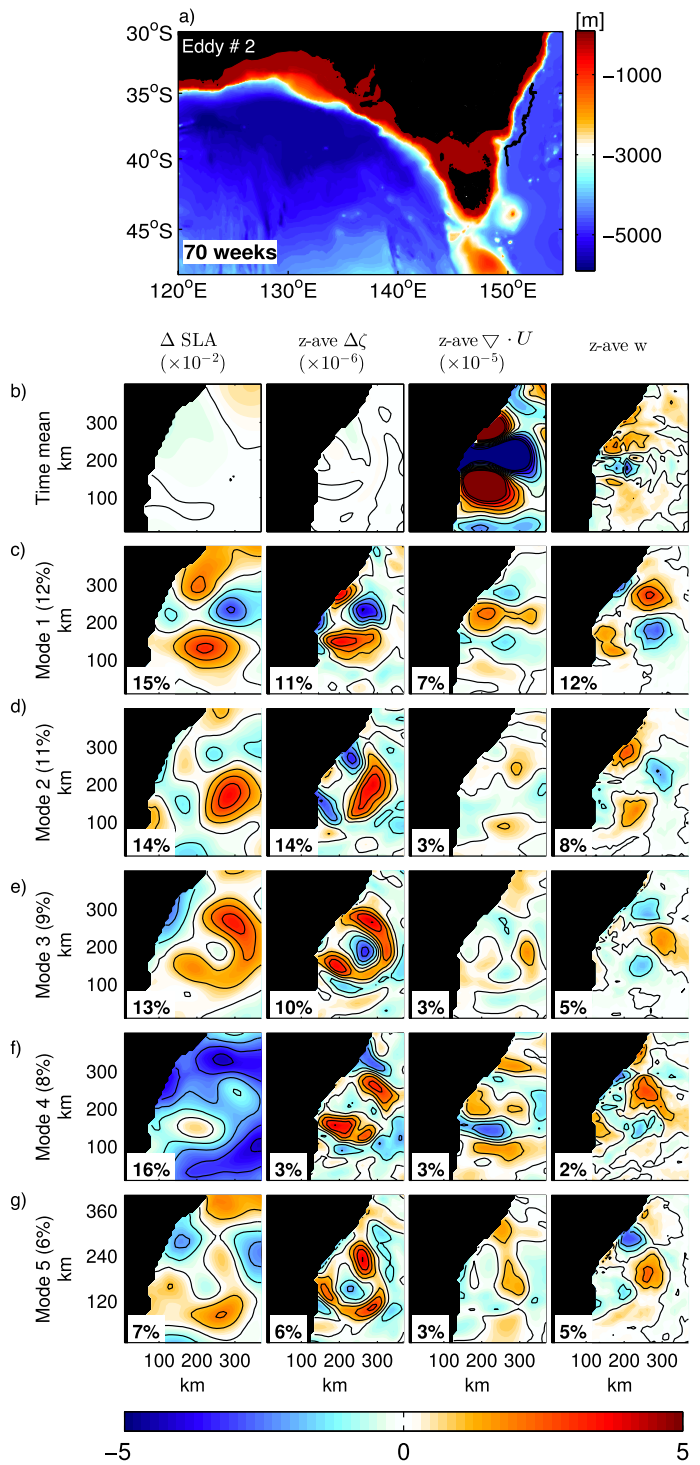

Figure 14. Same as in Figure 12, but for case study #2 propagating southward, off the eastern Australian shelf break.

We perform a multivariate EOF for eddy #1, to assess the coherence of the relationship between variables (Figure 12). For this analysis, we consider all time intervals of this eddy between southwest Tasmania and its dissipation (i.e., westward propagation; 91 weeks), and we follow the method described in section 2. The variables combined are ΔSLA, depth-averaged $\Delta\zeta_R$, depth-averaged $\nabla \cdot U$, and $\tilde{w}$. All the variables show the pattern of alternating cells in modes 2 and 3, resulting in up to 23% of the variance (Figures 12d and 12e). As seen in this eddy daily-averaged fieds, the ΔSLA and the $\Delta\zeta_R$ cells are directly related, and both are indirectly related to $\nabla \cdot U$ and $\tilde{w}$ cells. Therefore, both mechanisms are sustained as eddy #1 propagates westward in the Eastern Indian Ocean.

4.1.2. Eddy #2 Off Bass Strait

When eddy #2 is located off Bass Strait, it has a permanent pycnocline located at ∼500 m (Figure 10c). At this location, 65% of the horizontal velocity of the eddy is projected onto the barotropic mode, and 27% is projected onto the first baroclinic mode (Pilo et al., 2015). The dynamical changes associated with the eddy distortion in case study #1 also take place here. An inward distortion increases N^2 above the permanent pycnocline, is balanced by a negative $\Delta\zeta_R$, and results in upward motion (Figure 13; black section). Conversely, an outward distortion decreases N^2 above the permanent pycnocline, is balanced by a positive $\Delta\zeta_R$, and results in downward motion (Figure 13; magenta section).

For the time step shown in Figure 13, the relationship between divergence of the horizontal flow and ΔSLA is the opposite of the relationship suggested in section 4. Despite this opposing relationship, the volume within the eddy is still conserved. Here the outward distortion (i.e., in latitude) is associated with divergence (Figure 13e, magenta section), and the inward distortion (i.e., in longitude) is associated with convergence (Figure 13e, black section). To determine if this apparent inconsistency is true for other time steps of this eddy lifetime we again perform a multivariate EOF analysis of four variables (ΔSLA, $\Delta\zeta_R$, $\nabla \cdot U$, and $\tilde{w}$). For this analysis, we consider all time intervals of eddy #2 between its formation and south of Tasmania (i.e., southward propagation; 70 weeks). All the variables show the pattern of alternating cells in modes 1 and 2, summing up to 23% of the variance (Figures 14c and 14d). As suggested in section 4, the ΔSLA and the $\Delta\zeta_R$ cells are directly related, and both are indirectly related to $\nabla \cdot U$ and $\tilde{w}$ cells. Therefore, we conclude that, in the time interval chosen as a case study (i.e., when the eddy is off Bass Strait; Figures 10a, purple dot and 13), other forcings acted on the divergence pattern. These forcings might include eddy interaction with the bottom, with the mean flow, with other mesoscale features, and with the wind.

5. Discussion and Conclusion

We show that alternating cells of vertical velocity are a recurrent feature in anticyclonic eddies formed at the EAC separation region, as seen in a near-global, eddy-resolving model. These cells are most intense between 500 and 1,500 m depths, and are linked to eddy distortion, which is the change in eddy isotropy. These alternating upward and downward cells have been previously reported in cyclonic eddies of the Agulhas Return Current (Nardelli, 2013), in an eddy-dipole in the Iceland basin (Pidcock et al., 2013), and in an idealized anticyclonic eddy (Martin & Richards, 2001). In the eddies studied here, the alternating vertical velocity cells have magnitudes

of 10–50 m/d, with maximum values at middepth (500–1,500 m). These velocities are similar to 10–60 m/d vertical velocities, also stronger at middepth, reported in the literature (Martin & Richards, 2001; Nardelli, 2013; Pollard & Regier, 1992). The alternating upward and downward cells shown here rotate anticlockwise as the eddies propagate. A clockwise rotation of alternating upward and downward cells has also been reported in cyclonic eddies of the Agulhas Return Current (Nardelli, 2013, see their Figure 4).

While daily-averaged of vertical velocity within the modeled eddies of the EAC show four or more alternating cells, a time mean of this variable shows two cells only (Figures 4b, 12b, and 14b). These cells have downward velocity of 2 m/d at the leading part of the eddy, and upward velocity of the same magnitude in the trailing part of the eddy. This dual cell pattern is associated with the eddy propagation mechanism described by McGillicuddy et al. (1995). As in previous reports (e.g., Martin & Richards, 2001), the magnitude of the vertical velocity induced by eddy propagation in these eddies is 10 times smaller than the magnitude of the alternating upward and downward cells induced by eddy distortion. The hindering of the alternating upward and downward cells in a time-averaged eddy demonstrates the importance of studying eddies as case studies, and of considering their evolution at each time step.

We suggest two mechanisms to link the eddy distortion to vertical velocity. One mechanism relates to the conservation of the potential vorticity in the eddy, and the other, to the conservation of volume within the eddy. An analysis considering several time steps of the lives of two eddies suggests that these two mechanisms act together. However, in some moments of the eddy lifetime only one mechanism holds, as seen in the eddy off Bass Strait. These analyses show that the mechanisms linking eddy distortion and vertical velocity still require further discussion. Unanswered questions on this subject are: When is each mechanism more important than the other? And can the influence of these mechanisms in eddy vertical velocity be isolated?

We highlight three subjects for future investigation of vertical velocity within eddies. The first subject is the eddy distortion mechanism in cyclonic eddies and in Northern Hemisphere eddies. If using a global eddy-resolving model for such studies, we suggest the selected eddies to be coherent (i.e., no filaments), and isolated from other mesoscale features and the bottom. Here we demonstrate the importance of studying eddies as case studies. Only due to this approach, we were able to isolate the pattern of alternating vertical velocity and relate it to eddy distortion. The second subject is the reason for eddy distortion. For this investigation, we suggest using idealized eddies with different forcings (e.g., shear strain and eddy-bottom interaction). The third subject is the impact of the alternating upward and downward cells on primary productivity within the eddy. When exploring this subject, other dominant mechanisms that impact primary productivity within eddies must be kept in mind. These mechanisms include the eddy-Ekman pumping (Martin & Richards, 2001; Siegel et al., 2008), frontal submesoscale processes (Klein & Lapeyre, 2009), and eddy-bottom interaction (Oke & Griffin, 2011).

The vertical velocity within ocean eddies is a challenging research topic. Currently, the best tools to investigate this velocity are either outputs from ocean models, as used in this study, or vertical velocities calculated using the Omega equation. It would be useful to study vertical velocity within eddies in a global scale. Satellite altimetry provides this global coverage, and a 25 year temporal coverage. Here we show that the change in SLA fields is a good proxy for eddy distortion. We expect that future studies will be able to combine the methods shown here and to use the global, long term altimetry data to quantify eddy distortion and vertical velocity within eddies. Using altimetry fields to calculate eddy distortion would give us further information on submesoscale patterns, ageostrophic velocity, and the interior dynamics of ocean eddies. Ultimately, the connection between global satellite altimetry to the vertical velocity below could be used to construct a global estimate of vertical advection of nutrients, carbon, and other properties within oceanic eddies.

Acknowledgments

Gabriela S. Pilo acknowledges support by the CAPES Foundation, Brazilian Ministry of Education (grant 0520-13-6) and the Quantitative Marine Science PhD program from the University of Tasmania. The authors gratefully acknowledge input from Shane Keating, Hugo B. de Oliveira, Mark Baird, and two anonymous reviewers, that led to improvements of this work. OFAM was developed under Bluelink: a partnership between CSIRO, the Bureau of Meteorology and the Royal Australian Navy (http://wp.csiro.au/bluelink/, downloaded in January 2014). The Ocean Current altimeter products were produced by CSIRO and distributed by the Integrated Marine Observing System (http://oceancurrent.imos.org.au, downloaded in February 2014).

References

Allen, J., Smeed, D., Nurser, A., Zhang, J., & Rixen, M. (2001). Diagnosis of vertical velocities with the QG omega equation: An examination of the errors due to sampling strategy. *Deep Sea Research Part I: Oceanographic Research Papers*, *48*(2), 315–346. https://doi.org/10.1016/S0967-0637(00)00035-2

Alpine, J. E., & Hobday, A. J. (2007). Area requirements and pelagic protected areas: Is size an impediment to implementation? *Marine and Freshwater Research*, *58*(6), 558. https://doi.org/10.1071/MF06214

Baird, M. E., Suthers, I. M., Griffin, D. A., Hollings, B., Pattiaratchi, C., Everett, J. D., et al. (2011). The effect of surface flooding on the physical-biogeochemical dynamics of a warm-core eddy off southeast Australia. *Deep Sea Research Part II: Topical Studies in Oceanography*, *58*(5), 592–605. https://doi.org/10.1016/j.dsr2.2010.10.002

Biastoch, A., & Krauss, W. (1999). The role of mesoscale eddies in the source regions of the Agulhas Current. *Journal of Physical Oceanography*, *29*(9), 2303–2317. https://doi.org/10.1175/1520-0485(1999)029<2303:TROMEI>2.0.CO;2

Bowen, M. M., Wilkin, J. L., & Emery, W. J. (2005). Variability and forcing of the East Australian Current. *Journal of Geophysical Research*, *110*, C03019. https://doi.org/10.1029/2004JC002533

Brannigan, L. (2016). Intense submesoscale upwelling in anticyclonic eddies. *Geophysical Research Letters*, *43*, 3360–3369. https://doi.org/10.1002/2016GL067926

Brassington, G. B. (2010). Estimating surface divergence of ocean eddies using observed trajectories from a surface drifting buoy. *Journal of Atmospheric and Oceanic Technology*, *27*(4), 705–720. https://doi.org/10.1175/2009JTECHO651.1

Chelton, D. (2013). Mesoscale eddy effects. *Nature Geoscience*, *6*(8), 594–595. https://doi.org/10.1038/ngeo1906

Cresswell, G. R., & Legeckis, R. (1986). Eddies off southeastern Australia. *Deep Sea Research Part A. Oceanographic Research Papers*, *33*(11/12), 1527–1562. https://doi.org/10.1016/0198-0149(86)90066-X

Cushman-Roisin, B., Heil, W. H., & Nof, D. (1985). Oscillations and rotations of elliptical warm-core rings. *Journal of Geophysical Research*, *90*(C6), 11756. https://doi.org/10.1029/JC090iC06p11756

Dee, D., & Uppala, S. (2009). Variational bias correction of satellite radiance data in the ERA-Interim reanalysis. *Quarterly Journal of the Royal Meteorological Society*, *135*(644), 1830–1841. https://doi.org/10.1002/qj.493

Deng, X., Griffin, D. A., Ridgway, K. R., Church, J. A., Featherstone, W. E., White, N. J., et al. (2011). Satellite altimetry for geodetic, oceanographic, and climate studies in the Australian region. In *Coastal altimetry* (pp. 473–508). Berlin, Germany: Springer.

Dewar, W. K., & Flierl, G. R. (1987). Some effects of the wind on rings. *Journal of Physical Oceanography*, *17*, 1653–1667.

Ertel, H. (1940). Ein neuer hydrodynamischer Wirbelsatz. *Meteorologische Zeitschrift*, *59*, 277–281.

Everett, J. D., Baird, M. E., Oke, P. R., & Suthers, I. M. (2012). An avenue of eddies: Quantifying the biophysical properties of mesoscale eddies in the Tasman Sea. *Geophysical Research Letters*, *39*, L16608. https://doi.org/10.1029/2012GL053091

Flierl, G. R., & Mied, R. P. (1985). Frictionally induced circulations and spin down of a warm-core ring. *Journal of Geophysical Research*, *90*(C5), 8917–8927.

Fu, L., Chelton, D., Le Traon, P., & Morrow, R. (2010). Eddy dynamics from satellite altimetry. *Oceanography*, *23*(4), 14–25. https://doi.org/10.5670/oceanog.2010.02

Gaube, P., Chelton, D. B., Samelson, R. M., Schlax, M. G., & O'Neill, L. W. (2015). Satellite observations of mesoscale eddy-induced Ekman pumping. *Journal of Physical Oceanography*, *45*(1), 104–132. https://doi.org/10.1175/JPO-D-14-0032.1

Gaube, P., Chelton, D. B., Strutton, P. G., & Behrenfeld, M. J. (2013). Satellite observations of chlorophyll, phytoplankton biomass, and Ekman pumping in nonlinear mesoscale eddies. *Journal of Geophysical Research: Oceans*, *118*, 6349–6370. https://doi.org/10.1002/2013JC009027

Gill, A. E. (1982). *Atmosphere-ocean dynamics* (662 pp.). New York, NY: Academic Press.

Klein, P., & Lapeyre, G. (2009). The oceanic vertical pump induced by mesoscale and submesoscale turbulence. *Annual Review of Marine Science*, *1*(1), 351–375. https://doi.org/10.1146/annurev.marine.010908.163704

Lévy, M., Klein, P., & Treguier, A.-M. (2001). Impact of sub-mesoscale physics on production and subduction of phytoplankton in an oligotrophic regime. *Journal of Marine Research*, *59*(4), 535–565. https://doi.org/10.1357/002224001762842181

Ling, S. D., Johnson, C. R., Ridgway, K. R., Hobday, A. J., & Haddon, M. (2009). Climate-driven range extension of a sea urchin: Inferring future trends by analysis of recent population dynamics. *Global Change Biology*, *15*(3), 719–731. https://doi.org/10.1111/j.1365-2486.2008.01734.x

Mahadevan, A., Thomas, L. N., & Tandon, A. (2008). Comment on "Eddy/wind interactions stimulate extraordinary mid-ocean plankton blooms." *Science*, *320*(5875), 448b. https://doi.org/10.1126/science.1152111

Martin, A. P., & Richards, K. J. (2001). Mechanisms for vertical nutrient transport within a North Atlantic mesoscale eddy. *Deep Sea Research Part II: Topical Studies in Oceanography*, *48*, 757–773.

Mata, M. M., Wijffels, S. E., Church, J. A., & Tomczak, M. (2006). Eddy shedding and energy conversions in the East Australian Current. *Journal of Geophysical Research*, *111*, C09034. https://doi.org/10.1029/2006JC003592

McGillicuddy, D., & Robinson, A. (1997). Eddy-induced nutrient supply and new production in the Sargasso Sea. *Deep Sea Research Part I: Oceanographic Research Papers*, *44*(8), 1427–1450. https://doi.org/10.1016/S0967-0637(97)00024-1

McGillicuddy, D. J. (2015). Formation of intrathermocline lenses by eddy-wind interaction. *Journal of Physical Oceanography*, *45*(2), 606–612. https://doi.org/10.1175/JPO-D-14-0221.1

McGillicuddy, D. J., Anderson, L. A., Doney, S. C., & Maltrud, M. E. (2003). Eddy-driven sources and sinks of nutrients in the upper ocean: Results from a 0.1° resolution model of the North Atlantic. *Global Biogeochemical Cycles*, *17*(2), 1035. https://doi.org/10.1029/2002GB001987

McGillicuddy, D. J., Robinson, A. R., & McCarthy, J. J. (1995). Coupled physical and biological modelling of the spring bloom in the North Atlantic (II): Three dimensional bloom and post-bloom processes. *Deep Sea Research Part I: Oceanographic Research Papers*, *42*(8), 1359–1398. https://doi.org/10.1016/0967-0637(95)00035-5

McGillicuddy, D. J., Robinson, A. R., Siegel, D. A., Jannasch, H. W., Johnson, R., Dickey, T. D., et al. (1998). Influence of mesoscale eddies on new production in the Sargasso Sea. *Nature*, *394*(6690), 263–266. https://doi.org/10.1038/28367

McWilliams, J. C., Graves, L. P., & Montgomery, M. T. (2003). A formal theory for vortex Rossby waves and vortex evolution. *Geophysical & Astrophysical Fluid Dynamics*, *97*(4), 275–309. https://doi.org/10.1080/0309192031000108698

Nardelli, B. B. (2013). Vortex waves and vertical motion in a mesoscale cyclonic eddy. *Journal of Geophysical Research: Oceans*, *118*, 5609–5624. https://doi.org/10.1002/jgrc.20345

Nemcek, N., Ianson, D., & Tortell, P. D. (2008). A high-resolution survey of DMS, CO_2, and O_2/Ar distributions in productive coastal waters. *Global Biogeochemical Cycles*, *22*, GB2009. https://doi.org/10.1029/2006GB002879

Nilsson, C., & Cresswell, G. (1981). The formation and evolution of East Australian Current warm-core eddies. *Progress in Oceanography*, *9*(3), 133–183. https://doi.org/10.1016/0079-6611(80)90008-7

Nurser, A. J. G., & Zhang, J. W. (2000). Eddy-induced mixed layer shallowing and mixed layer/thermocline exchange. *Journal of Geophysical Research*, *105*(C9), 21851–21868. https://doi.org/10.1029/2000JC900018

Oke, P. R., & Griffin, D. A. (2011). The cold-core eddy and strong upwelling off the coast of New South Wales in early 2007. *Deep Sea Research Part II: Topical Studies in Oceanography*, *58*(5), 574–591. https://doi.org/10.1016/j.dsr2.2010.06.006

Oke, P. R., Griffin, D. A., Schiller, A., Matear, R. J., Fiedler, R., Mansbridge, J., et al. (2013). Evaluation of a near-global eddy-resolving ocean model. *Geoscientific Model Development*, *6*, 591–615. https://doi.org/10.5194/gmd-6-591-2013

Oliver, E. C. J., & Holbrook, N. J. (2014). Extending our understanding of South Pacific gyre "spin-up": Modeling the East Australian Current in a future climate. *Journal of Geophysical Research: Oceans*, *119*, 2788–2805. https://doi.org/10.1002/2013JC009591

Oliver, E. C. J., O'Kane, T. J., & Holbrook, N. J. (2015). Projected changes to Tasman Sea eddies in a future climate. *Journal of Geophysical Research: Oceans*, *120*, 7150–7165. https://doi.org/10.1002/2015JC010993

Olson, D. B. (1991). Rings in the ocean. *Annual Review of Earth and Planetary Sciences*, *19*, 283–311.

Pallas-Sanz, E., & Viudez, A. (2007). Three-dimensional ageostrophic motion in mesoscale vortex dipoles. *Journal of Physical Oceanography*, *37*(1), 84–105. https://doi.org/10.1175/JPO2978.1

Paterson, H. L., Knott, B., & Waite, A. M. (2007). Microzooplankton community structure and grazing on phytoplankton, in an eddy pair in the Indian Ocean off Western Australia. *Deep Sea Research Part II: Topical Studies in Oceanography*, *54*(8–10), 1076–1093. https://doi.org/10.1016/j.dsr2.2006.12.011

Pidcock, R., Martin, A., Allen, J., Painter, S. C., & Smeed, D. (2013). The spatial variability of vertical velocity in an Iceland basin eddy dipole. *Deep Sea Research Part I: Oceanographic Research Papers*, *72*, 121–140. https://doi.org/10.1016/j.dsr.2012.10.008

Pilo, G. S., Oke, P. R., Rykova, T., Coleman, R., & Ridgway, K. (2015). Do East Australian Current anticyclonic eddies leave the Tasman Sea? *Journal of Geophysical Research: Oceans*, *120*, 1–16. https://doi.org/10.1002/2015JC011026

Pollard, R. T., & Regier, L. A. (1992). Vorticity and vertical circulation at an ocean front. *Journal of Physical Oceanography*, *22*, 609–625. https://doi.org/10.1175/1520-0485(1992)022<0609:VAVCAA>2.0.CO;2

Reynolds, R. W., Smith, T. M., Liu, C., Chelton, D. B., Casey, K. S., & Schlax, M. G. (2007). Daily high-resolution-blended analyses for sea surface temperature. *Journal of Climate*, *20*(22), 5473–5496. https://doi.org/10.1175/2007JCLI1824.1

Ridgway, K., & Dunn, J. (2003). Mesoscale structure of the mean East Australian Current System and its relationship with topography. *Progress in Oceanography*, *56*(2), 189–222. https://doi.org/10.1016/S0079-6611(03)00004-1

Ridgway, K. R., Coleman, R. C., Bailey, R. J., & Sutton, P. (2008). Decadal variability of East Australian Current transport inferred from repeated high-density XBT transects, a CTD survey and satellite altimetry. *Journal of Geophysical Research*, *113*, C08039. https://doi.org/10.1029/2007JC004664

Rocha, C. B., da Silveira, I. C. A., Castro, B. M., & Lima, J. A. M. (2014). Vertical structure, energetics, and dynamics of the Brazil Current System at 22°S–28°S. *Journal of Geophysical Research: Oceans*, *119*, 52–69. https://doi.org/10.1002/2013JC009143

Roemmich, D., & Gilson, J. (2001). Eddy transport of heat and thermocline waters in the North Pacific: A key to interannual/decadal climate variability? *Journal of Physical Oceanography*, *31*, 675–687.

Roughan, M., Keating, S. R., Schaeffer, A., Cetina Heredia, P., Rocha, C., Griffin, D., et al. (2017). A tale of two eddies: The biophysical characteristics of two contrasting cyclonic eddies in the East Australian Current System. *Journal of Geophysical Research: Oceans*, *122*, 2494–2518. https://doi.org/10.1002/2016JC012241

Rykova, T., & Oke, P. R. (2015). Recent freshening of the East Australian Current and its eddies. *Geophysical Research Letters*, *42*, 9369–9378. https://doi.org/10.1002/2015GL066050

Rykova, T., Oke, P. R., & Griffin, D. A. (2017). A comparison of the structure, properties, and water mass composition of quasi-isotropic eddies in western boundary currents in an eddy-resolving ocean model. *Ocean Modelling*, *114*, 1–13. https://doi.org/10.1016/j.ocemod.2017.03.013

Siegel, D., Court, D., Menzies, D., Peterson, P., Maritorena, S., & Nelson, N. (2008). Satellite and in situ observations of the bio-optical signatures of two mesoscale eddies in the Sargasso Sea. *Deep Sea Research Part II: Topical Studies in Oceanography*, *55*(10–13), 1218–1230. https://doi.org/10.1016/j.dsr2.2008.01.012

Siegel, D. A., Peterson, P., McGillicuddy, D. J., Maritorena, S., & Nelson, N. B. (2011). Bio-optical footprints created by mesoscale eddies in the Sargasso Sea. *Geophysical Research Letters*, *38*, L13608. https://doi.org/10.1029/2011GL047660

Stern, M. E. (1965). Interaction of a uniform wind stress with a geostrophic vortex. *Deep Sea Research and Oceanographic Abstracts*, *12*, 355–367. https://doi.org/10.1016/0011-7471(65)90007-0

Strass, V. H. (1994). Mesoscale instability and upwelling. Part 2: Testing the diagnostics of vertical motion with a three-dimensional ocean front model. *Journal of Physical Oceanography*, *24*, 1759–1767. https://doi.org/10.1175/1520-0485(1994)024<1759:MIAUPT>2.0.CO;2

Suthers, I. M., Young, J. W., Baird, M. E., Roughan, M., Everett, J. D., Brassington, G. B., et al. (2011). The strengthening East Australian Current, its eddies and biological effects—An introduction and overview. *Deep Sea Research Part II: Topical Studies in Oceanography*, *58*(5), 538–546., https://doi.org/10.1016/j.dsr2.2010.09.029

Tilburg, C. E., Subrahmanyam, B., & O'Brien, J. J. (2002). Ocean color variability in the Tasman Sea. *Geophysical Research Letters*, *29*(10), 1487. https://doi.org/10.1029/2001GL014071

Tintoré, J., Gomis, D., Alonso, S., & Parrilla, G. (1991). Mesoscale dynamics and vertical motion in the Alboran Sea. *Journal of Physical Oceanography*, *21*, 811–823.

Tranter, D. J., Leech, G. S., & Vaudrey, D. J. (1982). Biological significance of surface flooding in warm-core ocean eddies. *Nature*, *297*(5867), 572–574. https://doi.org/10.1038/297572a0

Uysal, Z. (2006). Vertical distribution of marine cyanobacteria *Synechococcus* spp. in the Black, Marmara, Aegean, and eastern Mediterranean seas. *Deep Sea Research Part II: Topical Studies in Oceanography*, *53*(17–19), 1976–1987. https://doi.org/10.1016/j.dsr2.2006.03.016

Viudez, A., & Dritschel, D. G. (2003). Vertical velocity in mesoscale geophysical flows. *Journal of Fluid Mechanics*, *483*, 199–223. https://doi.org/10.1017/S0022112003004191

Waterman, S., & Jayne, S. R. (2011). Eddy-mean flow interactions in the along-stream development of a Western Boundary Current Jet: An idealized model study. *Journal of Physical Oceanography*, *41*(4), 682–707. https://doi.org/10.1175/2010JPO4477.1

Wyrtki, K., Magaard, L., & Hager, J. (1976). Eddy energy in the oceans. *Journal of Geophysical Research*, *81*(15), 2641–2646. https://doi.org/10.1029/JC081i015p02641